A LETTERS JOURNAL EXPLORING THE FRONTIERS OF PHYSICS

OFFPRINT

Modeling and simulation of mechanochemical processes in a rotational diamond anvil cell

V. I. LEVITAS and O. M. ZARECHNYY

EPL, **88** (2009) 16004

Please visit the new website
www.epljournal.org

A Letters Journal Exploring the Frontiers of Physics

October 2009

EPL, **88** (2009) 16004
doi: 10.1209/0295-5075/88/16004

www.epljournal.org

Modeling and simulation of mechanochemical processes in a rotational diamond anvil cell

V. I. Levitas[a] and O. M. Zarechnyy

Iowa State University, Departments of Mechanical Engineering, Aerospace Engineering, and Material Science and Engineering - Ames, IA 50011, USA

received 26 May 2009; accepted in final form 25 September 2009
published online 23 October 2009

PACS 64.60.-i – General studies of phase transitions

Abstract – Strain-induced structural changes (SCs), which include chemical reactions (CRs) and phase transitions (PTs), are studied here numerically under compression and torsion of a sample in a rotational diamond anvil cell (RDAC). The results change the fundamental understanding of the interpretation of experimentally observed effects and measurements and the extraction of information on material behavior from system (sample) behavior. These effects include the nontrivial, nonlinear interaction between strongly heterogeneous stress and plastic strain tensor fields and SC kinetics, the effect of change of material strength during SC, the simultaneous occurrence of direct and reverse SCs in different regions, strong strain localization, and pressure self-multiplication.

Copyright © EPLA, 2009

Mechanochemistry studies and utilizes various aspects of the effect of nonhydrostatic stresses and plastic strains on various SCs [1–5]. Mechanochemical processes are important for understanding earthquakes in geophysics, mechanochemical synthesis and alloying, processes during ball milling, high-velocity penetration problems, shock wave phase transformations and chemical reactions, shear ignition of explosives, and the search for new phases with unique properties. Pioneering studies on the unique mechanochemical behavior of materials under high pressure and large plastic strains in rotational Bridgman anvils [6–8] are now continued at a qualitatively new level in RDAC (see fig. 1) [9–14]. It is found that, because of the rotation of an anvil, the superposition of plastic shear under constant compressive load, leads to [4,5,9–14] 1) a drastic reduction (by a factor of 3–5) in SC pressure; 2) strain-controlled kinetics in which time is not significant and strain plays the role of a time-like parameter; 3) an appearance of new phases, that were not obtained without shear straining; 4) a reduction (up to zero) in pressure hysteresis; and 5) the replacement of a reversible SC by an irreversible SC, which allows one to use metastable phases in engineering applications under normal pressure. Results 1) and 4) have a preliminary character because they are obtained from complex experimental data that are not understood due to a lack of theory and simulations. Strain-induced SCs differ fundamentally from the similar pressure-induced SCs. For strain-induced SCs, phase-equilibrium pressure is not relevant, and the concept of SC pressure is not well defined because it depends up on plastic strain and the concentration c of the product phase. Mechanochemistry under compression and shear is a truly multiscale phenomenon. Our nano- and microscale theory [4,5,15] suggests that strain-induced SCs can be characterized in terms of pressure-dependent, strain-controlled kinetics, in which strain is a time-like parameter. However, SC kinetics can be experimentally determined in a macroscopic sample only. This was not done yet because it was suspected that the fields of stress and strain tensors and c are extremely heterogeneous; they strongly vary and interact with each other. These variations and interactions could not be measured. The measured radial pressure distribution along a diamond-sample contact surface [9–14] contains steps (plateaus) near a visible diffuse interface between low- and high-pressure phases, a pressure that was considered as PT or a phase-equilibrium pressure. However, the nature of these plateaus, as well as the meaning of these pressures for SC characterization, is not yet clear. Recently [9], we performed *in situ* X-ray diffraction measurement for PT in BN, which allowed us to determine radial distribution of concentration of the high-pressure phase averaged over the sample thickness. However, without knowledge of the distribution of stress and plastic strain tensors over the samples and the concentration of product phase over the sample thickness, which currently cannot be measured,

[a] E-mail: vlevitas@iastate.edu

it is impossible to quantitatively characterize and study strain-induced SCs. Thus, numerical modeling is the only way to determine these fields. This may lead to an iterative, numerical-experimental procedure to extract material properties and SC kinetics. The only work in this direction is devoted to the finite element method (FEM) study of plastic flow in RDAC but *without SC* [16]. A semi-qualitative analysis of SCs within a 1D model was performed in [4,5]. For DAC, plastic flow was studied in [17–21]. One of the basic equations for the analysis of DAC and RDAC experiments is the simplified equilibrium equation [4,5]

$$\mathrm{d}p/\mathrm{d}r = -2\tau_{rz}/h, \tag{1}$$

where $\mathrm{d}p/\mathrm{d}r$ is the radial pressure gradient, h is the sample thickness, and τ_{rz} is the radial shear (friction) stress at the contact surface between diamond and sample.

In this letter, we develop a model and a numerical approach and study the main features of coupled plastic flow and strain-induced SCs in RDAC in 3D formulation. A unified approach to strain-induced PT and CR is justified in [4,5]. The results of our nano- and microscale analysis [4,5,15] are included in the strain-controlled kinetic equation (5) and two characteristic pressures in it are of special importance: the minimum pressure p_ε^d, below which direct strain-induced SC is impossible, and the maximum pressure p_ε^r, above which reverse strain-induced SC is impossible. Very nonuniform fields of stress, strain, and plastic strain tensors, and c are determined for various loading programs, as well as for three ratios between yield strengths of parent σ_{y1} and product σ_{y2} phases. Various experimentally observed effects are reproduced and interpreted.

Model. – The deformation gradient tensor, $\boldsymbol{F} = \partial \boldsymbol{r}/\partial \boldsymbol{r}_0$, where $\boldsymbol{r} = \boldsymbol{r}(\boldsymbol{r}_0, t)$ and $\boldsymbol{r}_0$ are the locations of material points in the deformed state at time t and in the nondeformed state at $t = 0$, respectively, can be multiplicatively decomposed into elastic, transformational, and plastic parts, $\boldsymbol{F} = \boldsymbol{F}_e \cdot \boldsymbol{F}_t \cdot \boldsymbol{F}_p = \boldsymbol{V}_e \cdot \boldsymbol{R} \cdot \boldsymbol{F}_t \cdot \boldsymbol{F}_p$ [4,22]. Here, $\boldsymbol{R}$ characterizes the rigid-body rotation and $\boldsymbol{V}_e$ is the symmetric elastic stretch tensor. Representing $\boldsymbol{V}_e = \boldsymbol{I} + \boldsymbol{\varepsilon}_e$ and $\boldsymbol{F}_t = \boldsymbol{I} + \boldsymbol{\varepsilon}_t$, we will focus on the simplest case of a small elastic strain $\boldsymbol{\varepsilon}_e \ll \boldsymbol{I}$ and a small and pure volumetric transformation strain $\boldsymbol{\varepsilon}_t = \varepsilon_t/3\boldsymbol{I} \ll \boldsymbol{I}$, where $\boldsymbol{I}$ is the unit tensor, but large plastic strain and rotation. Then the total system of equations includes

$$\boldsymbol{d} = (\dot{\boldsymbol{F}} \cdot \boldsymbol{F}^{-1})_s = \overset{\nabla}{\boldsymbol{\varepsilon}}_e + \dot{\varepsilon}_t/3\boldsymbol{I} + \boldsymbol{d}_p; \tag{2}$$

$$\boldsymbol{T} = \boldsymbol{E} : \boldsymbol{\varepsilon}_e; \qquad \sigma_i \le \sigma_y(c); \qquad \sigma_y = (1-c)\sigma_{y1} + c\sigma_{y2}; \tag{3}$$

$$\boldsymbol{d}_p = \lambda \boldsymbol{s}; \qquad \varepsilon_t = \bar{\varepsilon}_t c; \qquad \boldsymbol{\nabla} \cdot \boldsymbol{T} = 0; \tag{4}$$

$$\frac{\mathrm{d}c}{\mathrm{d}q} = \frac{\frac{(1-c)}{a_{12}} \bar{p}_d H(\bar{p}_d) \frac{\sigma_{y2}}{\sigma_{y1}} - \frac{c}{a_{21}} \bar{p}_r H(\bar{p}_r)}{c + (1-c)\sigma_{y2}/\sigma_{y1}}. \tag{5}$$

Equation (2) is a decomposition of the deformation rate $\boldsymbol{d}$ into elastic, transformational, and plastic components, which follows from $\boldsymbol{F} = \boldsymbol{F}_e \cdot \boldsymbol{F}_t \cdot \boldsymbol{F}_p$; $\overset{\nabla}{\boldsymbol{\varepsilon}}_e = \dot{\boldsymbol{\varepsilon}}_e + 2(\boldsymbol{\varepsilon}_e \cdot \boldsymbol{W})_s$ is the Jaumann derivative, and $\boldsymbol{W} = (\dot{\boldsymbol{F}} \cdot \boldsymbol{F}^{-1})_a$ is the spin tensor; and subscripts s and a mean symmetric and skew-symmetric parts of a tensor. Equation $(3)_1$ is the elastic Hooke's law, with $\boldsymbol{T}$ for the true stress tensor and $\boldsymbol{E}$ for the isotropic elastic moduli tensor; eq. $(3)_2$ is the yield condition for isotropic, perfectly plastic material with $\sigma_i = (3/2\boldsymbol{s} : \boldsymbol{s})^{1/2}$ for stress intensity and $\boldsymbol{s}$ for deviatoric stress. Equation $(4)_1$ is the plastic flow rule with the scalar $\lambda = 0$ for $\sigma_i < \sigma_y$ (elastic regime) or as determined from the consistency condition $\dot{\sigma}_i = \dot{\sigma}_y$ for the plastic regime; $\bar{\varepsilon}_t$ is the volumetric transformation strain during SC; and eq. $(4)_3$ is the equilibrium equation. Equation (5) is the strain-controlled kinetic equation for SC [4,5,15], where q is the accumulated plastic strain ($\dot{q} := (2/3\boldsymbol{d}_p : \boldsymbol{d}_p)^{1/2}$), $\bar{p}_d = (p - p_\varepsilon^d)/(p_h^d - p_\varepsilon^d)$, $\bar{p}_r = (p - p_\varepsilon^r)/(p_h^r - p_\varepsilon^r)$, H is the Heaviside step function, p_h^d and p_h^r are pressures for direct and reverse SC under hydrostatic conditions, and σ_{y1} and σ_{y2} are yield strengths of the parent and product phases, and a_{ij} are the kinetic parameters.

Problem formulation. – The symmetry of the problem relative to horizontal plane BC passing through the sample center and the axis of rotation OB ($r = 0$) allows us to consider the quarter of the sample shown after deformation in fig. 1(a). At the OB and BC, radial shear stress $\tau_{rz} = 0$. Also, at BC the twisting and axial displacements are $u_\varphi = u_z = 0$. Then the half of the rotation angle $\varphi/2$ should be applied to the anvil. The initial thickness of the pre-indented part of a sample between flat diamond surfaces $h_0 = 0.1d = 0.5\bar{H}$, where d is the diameter of the anvil and $\bar{H}$ is the thickness of the nonindented part of the sample. To avoid any influence of the edge of the sample, we chose the diameter of the sample $D = 3d$.

Method. – The large elastoplastic deformation and coupled thermomechanical subroutines of the FEM code ABAQUS [23] were implemented, in which the transformation strain was modeled through the thermal strain. Concentration c was treated as the temperature, and the subroutine for the thermal conduction equation with zero thermal conductivity and heat sources according to eq. (5) was used to solve kinetic equation eq. (5). An axisymmetric geometrical model with 3D loading was utilized, and compressive force and rotation angle (or torque) were applied to the analytical rigid surface, which modeled the diamond. We simulated material compression by the axial force F (applied at the center of the RDAC (fig. 1)), followed by torsion at $F = \mathrm{const}$ and reduction of F, followed by torsion at $F = \mathrm{const}$. The loading path was divided into a number of steps, and after each step the ABAQUS built-in remeshing procedure was performed. Pressure and shear stresses are divided by σ_{y1} and the yield strength in shear τ_{y1}, respectively, and axial force F is normalized by initial contact area and σ_{y1}.

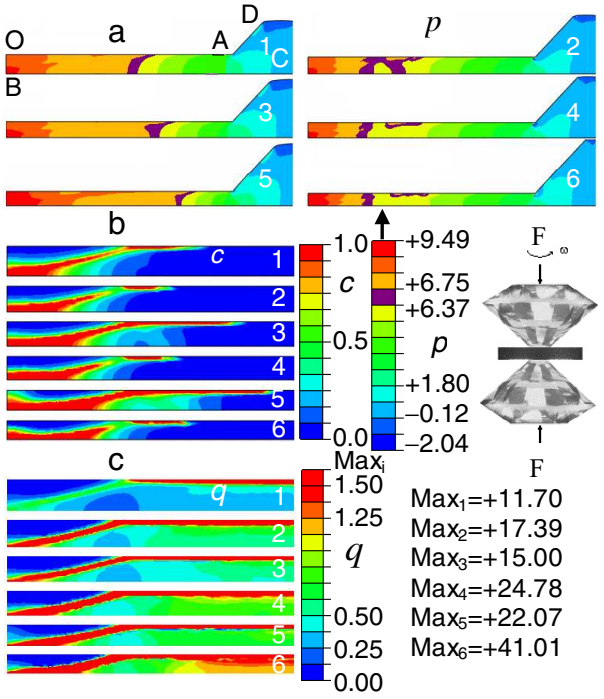

Fig. 1: (Color online) Comparison of distributions of pressure p (a), concentration of high-pressure phase c (b), and accumulated plastic strain q (c) for compression (1, 3, 5) and torsion (2, 4, 6) for $\sigma_{y2} = 0.2\sigma_{y1}$. The pressure at the contact surface at $r = 0$ after pure compression and torsion is the same and equal to 7.95 (1 and 2), 8.10 (3 and 4), and 8.80 (5 and 6). The axial force F is 5.07 (1), 5.42 (3), 6.11 (5), and 4.44 (2, 4, 6). The rotation angle φ is 0.20 (2), 0.32 (4), and 0.64 (6). Pressure legends are uniform with exception of the inserted pressure range $p_\varepsilon^r < p < p_\varepsilon^d$ (magenta), in which SCs do not occur. Max$_i$ designates the maximum value of q in otherwise uniform legends. The inset shows the schematics of the rotational diamond anvil cell.

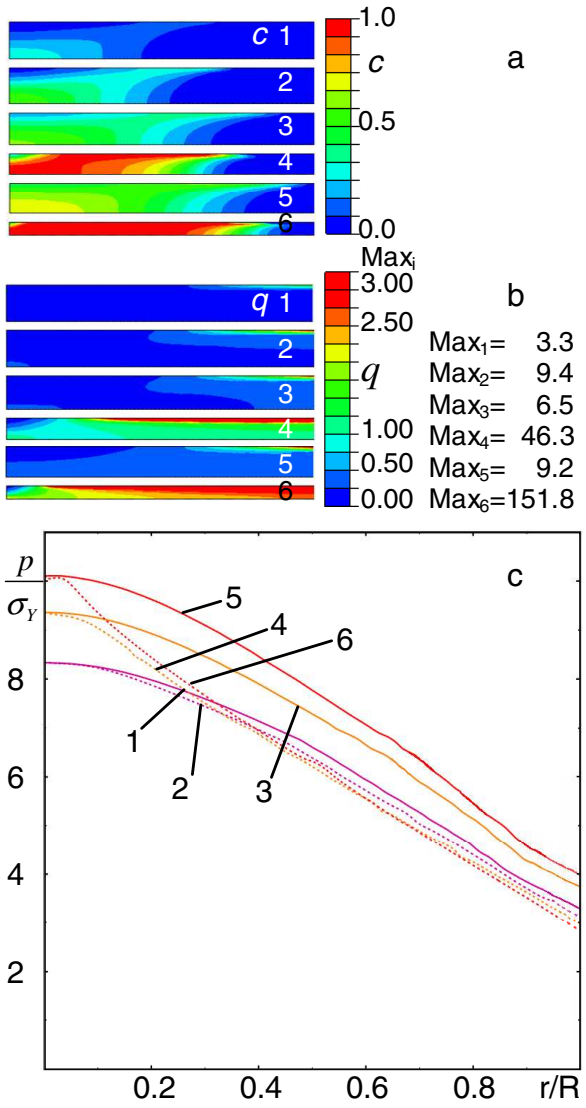

Fig. 2: (Color online) Comparison of distributions of concentration of the high-pressure phase c (a), accumulated plastic strain q (b), and pressure p (c), for compression (1, 3, 5) and torsion (2, 4, 6) for $\sigma_{y2} = \sigma_{y1}$. The pressure at the contact surface at $r = 0$ after pure compression and torsion is the same and equal to 8.40 (1 and 2), 9.40 (3 and 4), and 10.2 (5 and 6). The axial force F is 4.46 (1), 5.04 (3), 5.43 (5), and 4.44 (2, 4, 6). The rotation angle φ is 0.04 (2), 0.60 (4), and 1.57 (6).

The following material parameters were used: $p_\varepsilon^d = 6.75$, $p_\varepsilon^r = 6.375$, $p_h^d = 11.25$, $p_h^r = 1.875$, $a_{ij} = 0.1$, Young modulus $E = 162.5$, and Poison's ratio $\nu = 0.3$.

Results. – Comparisons of the fields p, q, and c after compression and after torsion for three strength ratios are presented in figs. 1–3.

Torsion was performed at force $F = 4.44$, and compression without torsion was performed to the same pressure at the sample center as it was for the case with torsion. For all cases, SC starts at the center of the sample, where pressure first exceeds p_ε^d and where some strain localization occurs along the slip line passing through the center of a sample. For all cases, another local maximum in c appears along the contact surface in the region with very large plastic strain. For $\sigma_{y2} = 5\sigma_{y1}$ during torsion, pressure grows significantly at the center of a sample, despite the volume decrease due to SC, which corresponds to the experimentally observed pressure self-multiplication effect [9–12]. The reduction in thickness due to torsion compensates the SC-induced volume decrease, and higher yield strength leads to pressure growth.

For all cases except compression with torsion for $\sigma_{y2} = 0.2\sigma_{y1}$, SC in both SC regions completes, and these zones coalesce; for $\sigma_{y2} \geqslant \sigma_{y1}$, SC completes in almost the entire part of a sample where $p > p_\varepsilon^d$. For $\sigma_{y2} = 0.2\sigma_{y1}$, for compression and compression and torsion, plastic strain strongly localizes in the transformed region because of the reduction in strength. However, for the case with torsion, two transformed regions are separated by a low-pressure zone with $p < p_\varepsilon^d$, so that they cannot grow and coalesce (fig. 1). Thus, distribution of c is very heterogeneous. When the yield strength is reduced during the SC, the simplified model [4,5] suggests a significant pressure drop

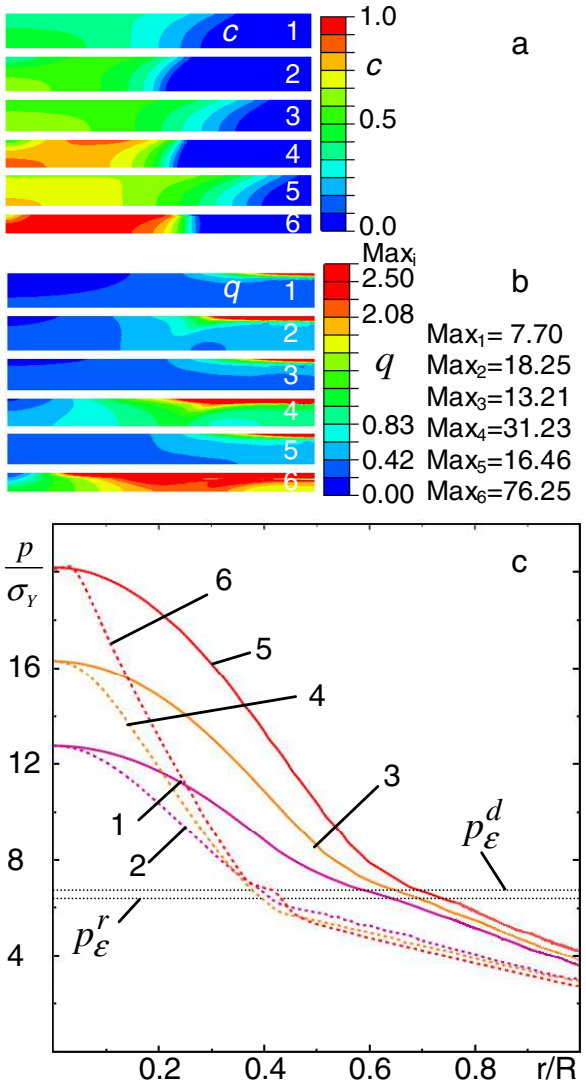

Fig. 3: (Color online) Comparison of distributions of concentration of the high-pressure phase c (a), accumulated plastic strain q (b), and pressure p (c), for compression (1, 3, 5) and torsion (2, 4, 6) for $\sigma_{y2} = 5\sigma_{y1}$. The pressure at the contact surface at $r = 0$ after pure compression and torsion is the same and equal to 12.4 (1 and 2), 16.2 (3 and 4), and 20.1 (5 and 6). The axial force F is 5.47 (1), 6.26 (3), 7.21 (5), and 4.44 (2, 4, 6). The rotation angle φ is 0.20 (2), 0.52 (4), and 1.11 (6).

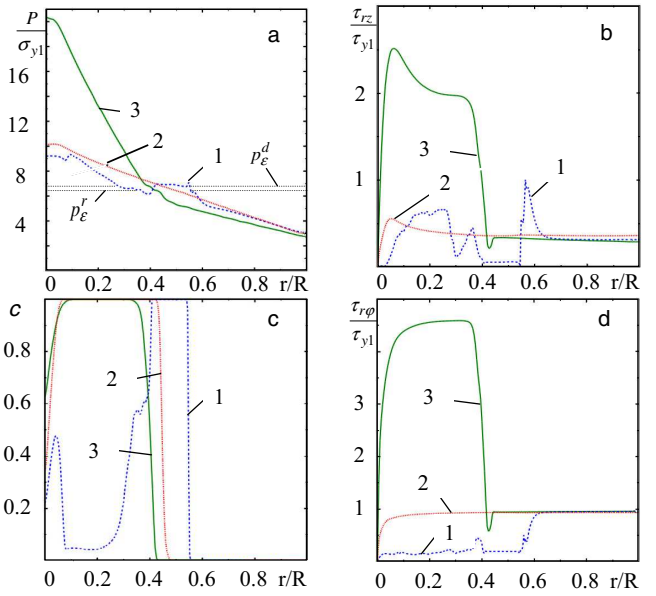

Fig. 4: (Color online) Distributions of pressure, shear stresses τ_{rz} and $\tau_{r\varphi}$ and c along the contact surface for the rotation angle $\varphi = 0.65$ and $\sigma_{y2} = \sigma_{y1}$ (red dotted line (2)), $\sigma_{y2} = 0.2\sigma_{y1}$ (blue dashed line (1)), and $\sigma_{y2} = 5\sigma_{y1}$ (solid green line (3)).

in the SC region. However, our FEM simulations show that in the completely transformed zone near the contact surface the pressure grows. At the center of a sample, where the pressure is maximum, it decreases slightly, then increases. All of these surprising results are due to nontrivial, nonlinear interaction between SC, plastic flow, and stress redistribution, which could not be described by a simplified model.

Because during torsion the thickness of a sample is intensively reduced and the high-pressure phase radially flows to the low-pressure region, strain-induced reverse SCs start. Thus, both direct and reverse SCs occurs simultaneously in different regions. If the kinetics of the reverse SC is slow, the high-pressure phase may be found at a low pressure, at which it cannot be obtained due to SC, leading to an incorrect interpretation of the SC pressure.

Another important result is that experimentally observed plateaus (steps) in the pressure-distribution curve have been reproduced in our calculation (fig. 4). For $\sigma_{y2} = 5\sigma_{y1}$, the plateau under torsion corresponds to the diffuse interface (two-phase region) between completely transformed and nontransformed material (as was observed in experiments for KCl and fullerene C_{60} [10–12]). For $\sigma_{y2} = 0.2\sigma_{y1}$, however, the plateau appears in the ring corresponding to a completely transformed material near the diamond-sample contact surface, both for compression and for compression and torsion.

It was suggested earlier that the pressure value at these steps can be used as the pressure characterizing the SC, in particular phase-equilibrium pressure (see, *e.g.*, [10]). One of the arguments was that a zero pressure gradient corresponds to zero shear stress (eq. (1)) *i.e.*, to hydrostatic condition. In addition, plastic strain reduces plastic hysteresis, and because in [10] hysteresis was zero, then pressure at the step is the phase-equilibrium pressure. The inconsistency of this consideration is discussed in [4,5] and is related to the fundamental difference between pressure-induced and strain-induced SCs; however, interpretation of the pressure at the step was still unknown. Among possible reasons for a zero pressure gradient are zero yield strength in the SC region (which is wrong [4,5]), transformation-induced plasticity, and zero radial velocity due to volume decrease during SC [4,5]. However, current FEM simulations have demonstrated that none of the

above reasons is true because $\tau_{rz} \neq 0$ (fig. 4). Results show that eq. (1) is not applicable in the region with a large concentration gradient, and that is why it leads to incorrect conclusions and interpretations. It is also not applicable for $\sigma_{y2} < \sigma_{y1}$ in the entire sample due to strain localization —compare $p(r)$ and τ_{rz} in fig. 4.

For torsion and $\sigma_{y2} > \sigma_{y1}$, pressure at steps slightly varies between p_ε^d and p_ε^r, which can be connected with the plastic flow of phase 2 in the low-pressure regions. Indeed, if, due to the reduction in thickness of a sample during the torsion, the high-pressure phase flows radially in the region with $p < p_\varepsilon^d$, and its reverse transformation will not start until it reaches the radius at which $p < p_\varepsilon^r$. Under intense SCs, a diffuse interface locates in the ring corresponding to the pressure range $p_\varepsilon^r < p < p_\varepsilon^d$. This result allows us to approximately identify these two key material parameters from a torsion experiment. Torsion leads to a sharper interface, which corresponds to experiments on KCl [10].

Note that in experiments, plateaus are observed during compression as well and pressure at the plateaus is reduced after torsion. However, we did not observe plateaus under compression for $\sigma_{y2} \geqslant \sigma_{y1}$, which may be because of relatively slow kinetics or some missing physics in the model. On the other hand, there is a plateau under compression for $\sigma_{y2} = 0.2\sigma_{y1}$ when SC is completed at the contact surface, which is above the plateau after torsion —*i.e.*, as in experiments for PT ZnSe [13] and CuI [14]. However, the simulated pressure at the plateau under compression does not correspond to any characteristic pressure, and the interpretation of such an experimentally determined pressure is not clear. Also, a plateau under torsion corresponds to p_ε^d when c reached 1 at the contact surface. Further rotation leads to a pressure increase at the plateau, which is not related to SC, because it is completed. In fig. 4(a), there are several steps on the $p(r)$ curve corresponding to p_ε^d and p_ε^r. Because SC can occur at any pressure above p_ε^d, it looks as though pressure at the plateau (when it is not related to p_ε^r and p_ε^d) is determined by the mechanics of plastic flow with SC rather than by SC-related characteristics.

We conclude that for torsion and $\sigma_{y2} > \sigma_{y1}$, pressure at steps slightly varies between p_ε^d and p_ε^r and can be used to determine these important pressures from experiment. Thus, for KCl, $p_\varepsilon^d \simeq p_\varepsilon^r \simeq 1.8\,GPa$, based on experiments in [10]. For torsion and $\sigma_{y2} < \sigma_{y1}$, the steps and plateau correspond to p_ε^d and p_ε^r, but it is not easy to distinguish them from steps and plateaus that are not related to SC parameters. For compression, pressure at the plateau does not correspond to any characteristic SC pressure, and this is probably true for compression for any σ_y because pressure at steps varies during plastic loading. Thus, the statement that plastic shear reduces the SC pressure, while generally correct, is not justified when it is based on a reduction in pressure at steps during torsion.

When comparing cases with and without torsion, one needs to remember that (in contrast to hydrostatic loading) strain-induced SCs occur for both loadings. Thus, the physics, thermodynamics, and kinetics are the same, with only the *p-q* paths at each point differing. We will compare parameters for completion of the SC at the contact surface. Torsion was performed under $F = 4.44$, but loadings for compression are different from those in figs. 1–3. For $\sigma_{y1} = \sigma_{y2}$, SC occurs in the region $r/R < 0.65$ at maximum $p = 14.3$ and $F = 5.5$ under compression and in the region $r/R < 0.38$ at $p = 9.4$ and $\varphi = 0.6$ for torsion. For $\sigma_{y2} = 5\sigma_{y1}$, complete SC occurs in the region $r/R < 0.6$ at $p = 53$ and $F = 12.29$ under compression and in the region $r/R < 0.32$ at $p = 20$ and $\varphi = 1.11$ for torsion. For $\sigma_{y2} = 0.2\sigma_{y1}$, it occurs in the ring $0.3 < r/R < 0.7$ at $p = 8.3$ and $F = 5.5$ under compression and in the ring $0.35 < r/R < 0.55$ at $p = 9.6$ and $\varphi = 1.40$ for torsion. Thus, torsion significantly reduces the maximum pressure in a sample for complete SC for $\sigma_{y2} = \sigma_{y1}$, and especially for $\sigma_{y2} = 5\sigma_{y1}$, which is important if the experiment is performed at the limit of diamond strength. However, the region in which SC occurs is reduced due to torsion. Because thickness during the torsion is reduced as well, the high-pressure phase volume is reduced even more. Surprisingly, torsion suppresses SC for $\sigma_{y2} = 0.2\sigma_{y1}$ —*i.e.*, it reduces the volume of the high-pressure phase and increases the maximum pressure in the sample for transformation. Complete SC under torsion occurs in two regions that do not coalesce, while under compression they coalesce and become significantly larger (fig. 1).

Distributions of pressure, shear stresses τ_{rz} and $\tau_{r\varphi}$, and c along the contact surface are shown in fig. 4 for $\varphi = 0.65$ and three yield strength ratios. Important features are 1) a sharp change in τ_{rz} and $\tau_{r\varphi}$ at a diffuse interface, and 2) that $\sqrt{\tau_{rz}^2 + \tau_{r\varphi}^2}$ in a single-phase region reaches a corresponding yield strength normalized by τ_{y1} in the major part of a sample. Shear stress τ_{rz} does not change the sign, so there is no flow to the center of a sample. This is *in contrast* to generally accepted knowledge based on eq. (1) that pressure maximum corresponds to zero sliding velocity and that material flows radially in the direction of the pressure gradient [4,5,13]. However, a drop in shear stresses is observed at the interface. While for $\sigma_{y2} \geqslant \sigma_{y1}$ the pressure distribution is smooth, it is very irregular for $\sigma_{y2} < \sigma_{y1}$. This is confirmed by a smooth, measured pressure distribution in KCl [10,11] and fullerene [11,12] and by an irregular pressure distribution in ZnSe [13] and CuI [14]. A slight increase in pressure at the center during PT in ZnSe [13] under torsion correlates with our results for $\sigma_{y2} < \sigma_{y1}$.

For *unloading*, a reduction in F causes both direct and reverse SC in two-phase region at the initial stage and then reverse SC only. Thus, it is accompanied by plastic straining. For $\sigma_{y2} = 5\sigma_{y1}$, after reduction in F by 30%, torsion by $\varphi = 0.1$ causes an irregular drop in c, while torsion by $\varphi = 1$ leads to a sharp interface. A plateau corresponding to p_ε^r appears starting with a reduction of F by 20% and remains during torsion. Thus, unloading

followed by torsion is a promising way to determine p^r_ε experimentally.

Conclusions. – 3D model is developed, and FEM simulations of SC in RDAC are performed. The results lead to change in the basic understanding of interpretation of experimentally observed effects and measurements and the extracting of information on material behavior from the sample behavior. They also represent a tool for designing experiments for different purposes and for controlling SCs. We found that in the regions with strong gradients of concentration of phases (at the plateaus) and (in the case of weaker product phases) in the entire sample, eq. (1) leads to incorrect results, which caused major confusion in the field. Thus, there is no drop in shear stress τ_{rz} to zero at the plateaus, for $\sigma_{y2} = 0.2\sigma_{y1}$ pressure in transformed regions does not drop, the pressure maximum at the contact surface does not always correspond to zero sliding velocity, and material does not always flow radially in the direction of the pressure gradient. Experimentally observed plateaus in the pressure-distribution curve have been reproduced. For $\sigma_{y2} = 5\sigma_{y1}$, the plateau indeed corresponds to the diffuse boundary (two-phase region) between completely transformed and nontransformed material. Pressure at steps varies slightly between p^d_ε and p^r_ε, which allows to identify these two key material parameters through experiment. For $\sigma_{y2} = 0.2\sigma_{y1}$, calculations reproduce an experimentally observed, highly irregular pressure field and plateau, and suggest when it is possible to extract p^d_ε and p^r_ε and when pressure at steps does not have any specific meaning for strain-induced SC. It is surprising, but in this case torsion does not promote the SC in comparison with compression. Unloading followed by torsion is a promising way to determine p^r_ε experimentally. Under loading, when product phase is stronger than the parent phase, pressure grows strongly during the torsion and SC, despite the volume decrease due to SC. This result is not in contradiction with the Le Chatelier principle because the thermodynamics of heterogeneous, strain-induced SCs differs significantly from classical thermodynamics [4,5], corresponding instead to the experimentally observed pressure self-multiplication effect [9–12]. Also, during torsion, the thickness of a sample is reduced, and the high-pressure phase radially flows to the low-pressure region, where strain-induced reverse SCs start. Thus, both direct and reverse SCs occur simultaneously in different regions. Obtained results open ways to extract information on material properties and SC kinetics by coupling simulations and experiment, as well as to control SC by controlling the loading path.

Our conclusion may be broadened when we change the kinetic coefficient or the entire equation, take $p^r_\varepsilon > p^d_\varepsilon$, consider torsion at a lower load when plastic flow does not start at the center of a sample during compression, and use a gasket. Due to the strong heterogeneity of all fields, especially q and c, it is difficult to extract the kinetic equation for SCs eq. (5) from an experiment. In [9] we predicted theoretically and confirmed experimentally the method for creating a quasi-homogeneous pressure distribution in a sample by designing sample and gasket geometry. As a result, $c(r)$ was also quasi-homogeneous. A FEM study of this problem will be performed in the future.

* * *

ARO, DTRA, ISU, and TTU support is gratefully acknowledged.

REFERENCES

[1] Gilman J. J., *Science*, **274** (1996) 65.
[2] Kim J. J., Choi Y., Suresh S. and Argon A. S., *Science*, **295** (2002) 654.
[3] Hickenboth C. R., Moore J. S., White S. R., Sottos N. R., Baudry J. and Wilson S. R., *Nature*, **446** (2007) 423.
[4] Levitas V. I., *High Pressure Surface Science and Engineering*, edited by Gogotsi Y. and Domnich V. (IOP, Bristol) 2004, sect. 3, pp. 159–292.
[5] Levitas V. I., *Phys. Rev. B*, **70** (2004) 1.
[6] Bridgman P. W., *Phys. Rev.*, **48** (1935) 825.
[7] Enikolopyan N. S., *Russ. J. Phys. Chem.*, **63** (1989) 2289.
[8] Zharov A. A., *Usp. Khim.*, **53** (1984) 236.
[9] Levitas V. I., Ma Y., Hashemi J., Holtz M. and Guven N., *J. Chem. Phys.*, **125** (2006) 044507.
[10] Blank V. D., Boguslavski Yu. Ya., Eremetz M. I., Izkevich E. S., Konyaev Yu. S. *et al.*, *Sov. Phys. JETP*, **87** (1984) 922.
[11] Novikov N. V., Polotnyak S., Shvedov L. and Levitas V. I., *J. Superhard Mater.*, **3** (1999) 39.
[12] Blank V. D., Buga S.G., Popov M. Y., Davydov V. A., Agafonov V. *et al.*, *New J. Chem.*, **19** (1995) 253.
[13] Blank V. D. and Buga S. G., *Instrum. Exp. Tech.*, **36** (1993) 149.
[14] Batsanov S. S., Serebryanaya N. R., Blank V. D. and Ivdenko V. A., *Crystallogr. Rep.*, **40** (1995) 650.
[15] Levitas V. I. and Zarechnyy O. M., *J. Phys. Chem. B*, **110** (2006) 16035.
[16] Levitas V. I. and Zarechnyy O. M., *Appl. Phys. Lett.*, **91** (2007) 141919.
[17] Moss W. C., Hallquist J. O., Reichlin R., Goettel K. A. and Martin S., *Appl. Phys. Lett.*, **48** (1986) 125.
[18] Weir S. T., Akella J., Ruddle C., Goodwin T. and Hsiung L., *Phys. Rev. B*, **58** (1998) 11258.
[19] Merkel S., Hemley R. J. and Mao H. K., *Appl. Phys. Lett.*, **74** (1999) 656.
[20] Novikov N. V., Levitas V. I. and Idesman A. V., *High Pressure Res.*, **5** (1990) 868.
[21] Levitas V. I., Polotnyak S. B. and Idesman A. V., *Strength Mater.*, **3** (1996) 221.
[22] Levitas V. I., *Int. J. Solids Struct.*, **35** (1998) 889.
[23] ABAQUS Hibbit Karlsson and Sorensen Inc. Ver. 6.2, 2001.